Applied Catalysis B: Environmental 322 (2023) 122125

Contents lists available at ScienceDirect

Applied Catalysis B: Environmental

journal homepage: www.elsevier.com/locate/apcatb

One-pot non-covalent heterogenization and aromatization of poly(ionic liquids) for metal-/cocatalyst-free and atmospheric CO_2 conversion

Mingyue Qiu [a,1], Jie Li [b,1], Haonan Wu [a], Yi Huang [a], Huijuan Guo [a], Dan Gao [c], Lijuan Shi [a,*], Qun Yi [a,d,**]

[a] School of Chemical Engineering and Pharmacy, Wuhan Institute of Technology, Wuhan 430205, PR China
[b] State Key Laboratory of Clean and Efficient Coal Utilization, Taiyuan University of Technology, Taiyuan 030024, PR China
[c] School of Energy, Power and Mechanical Engineering, North China Electric Power University, Beijing 102206, PR China
[d] Shanxi-Zheda Institute of Advanced Materials and Chemical Engineering, Taiyuan 030024, PR China

ARTICLE INFO

Keywords:
CO_2 activation
Metal-free
Aromatization
Dynamic imine assembly
Poly(ionic liquid)

ABSTRACT

The intensification of Lewis acidity/basicity of a given heterogeneous catalyst at a molecular level is an advanced approach for boosting CO_2 activation and conversion under extremely mild conditions, which, yet remains a great challenge. This work proposes a one-pot strategy for heterogenization and aromatization of homopolymerized ionic liquids (HpolyILs) through dynamic imine assembly with aromatic spacers for boosting CO_2 conversion into cyclic carbonates. The aromatization of HpolyILs can be controllably achieved at room temperature, and has been proven to enhance the Lewis acidity of C-2 proton on imidazolium IL for promoting ring-opening of epoxides and facilitate CO_2 bending synchronously. The resultant dynamic covalent polyILs exhibit superior catalytic activity and outstanding recyclability for a variety of epoxides under extremely mild conditions (1 atm, 50–90 °C) without metal/co-catalyst consumption. This work offers a feasible to scale-up approach for tailor-made designing high-efficiency heterogeneous catalysts for CO_2 utilization, guiding the precise regulation of acid-base catalysis.

1. Introduction

CO_2 conversion into high value-added products under atmospheric conditions is of vital meaning for CO_2 emission reduction in terms of climate protection and resource utilization [1,2]. Particularly, the coupling reaction of CO_2 and epoxides to synthesize cyclic carbonates has been considered as a promising route for CO_2 conversion because of the 100% atom utilization rate and wide application of the products [3–5]. Due to the high energy barrier of the ring-opening step of epoxides (the rate-determining step in such class of reaction) [6], great efforts have been made for developing efficient catalysts (especially heterogeneous ones). Most of the reported catalysts, nevertheless, still suffer from low catalytic activity (high reaction temperature and/or high CO_2 pressure) and/or high cost (i.e., complex synthesis, metal/-solvent/cocatalyst consumption) [2,7–10]. Very recently, focus has been paid to the nature of catalytic mechanism, and Lewis acidic or basic sites have been demonstrated to facilitate the rate determining step (i.e., the ring-opening of epoxides) through electrostatic attraction [11], ion-dipole [12–14] or hydrogen bonding [15]. It is therefore of great significance if one can manipulate the nature of active sites (i.e., strength, content and spatial location [16,17]) in a given heterogeneous catalyst to promote the catalytic activity under extremely mild conditions (even at room temperature or atmospheric pressure).

Ionic liquids (ILs) possess nucleophilic anions (e.g., halide ions) and acidic sites (e.g., C-2 proton on imidazolium ring), performing intrinsic activity for attacking epoxides and interacting with CO_2 molecules [18]. The flexible designability of ILs provides a feasible platform to precisely design and regulate the Lewis acidity/basicity at a molecular level [19,20]. Nevertheless, the homogeneous nature, i.e., high viscosity and difficulty in separation has led to great focus on the heterogenization of IL. The most popular heterogenization approach until now is the post-synthesis covalent grafting of ILs on rigid porous nanomaterials [21–25], wherein low IL load and especially fixed location in rigid skeleton hinders the cooperation of active sites for generating a

* Corresponding author.
** Corresponding author at: School of Chemical Engineering and Pharmacy, Wuhan Institute of Technology, Wuhan 430205, PR China
E-mail addresses: shilijuanwit@sina.com (L. Shi), yq20071001@163.com (Q. Yi).
[1] These authors contributed equally to this work.

https://doi.org/10.1016/j.apcatb.2022.122125
Received 8 August 2022; Received in revised form 6 October 2022; Accepted 26 October 2022
Available online 28 October 2022

competitive catalytic activity under mild conditions. Alternatively, polymerization of ILs can ensure an enriched content of ILs and the flexibility of polymers, enabling a desirable spatial close of active sites to cooperate with each other during the catalytic process [2,26–29]. Nevertheless, homopolymerized ILs generally exhibit thick liquid or gel state and maintain homogeneous nature in the coupling reaction of CO_2 and epoxides [29]. The incorporation of aromatic backbone into flexible polymers is of high promise for the heterogenization of poly(ionic liquids) (polyILs) [2,26,28,29]. Moreover, the rigid skeleton ensures an efficient access of active sites with substrates, thus counterbalancing the utilization efficiency and cooperation effect of active sites [27]. Meanwhile, the incorporation of electron-withdrawing aromatic group is hopeful for facilitating CO_2 activation [30]. Considering complex covalent synthesis procedure is often required during the copolymerization of IL and aromatic monomers, great challenges remain to explore a facile and green approach for the facile heterogenization and aromatization of homopolymerized ILs.

Dynamic covalent chemistry (DCC) involves a series of covalent chemical reactions in reversible equilibrium that are based on dynamic covalent bonding (e.g., ester bonding, imine bonding, acylhydrazone bonding, and bisulfide bonding) [31–33]. As a typical class of dynamic covalent bonds, dynamic imine bond can undergo reversible reactions under mild conditions and possesses specific directionality and robustness, endowing the assemblies with high stability and recyclability [34]. Herein, we propose a dynamic covalent strategy for the heterogenization and aromatization of homopolymerized imidazolium ILs through imine assembly with aromatic spacers. By virtue of the dynamic non-covalent nature, the structure of the dynamic covalent heterogenous polyILs can be facilely regulated through the assembly process control, thus offering a feasible approach for promoting the catalytic activity. The incorporation of aromatic moiety has been proven to bend CO_2 and promote the hydrogen bonding between C-2 proton on imidazolium ring and O on epoxides synchronously, thus boosting the reaction of CO_2 and epoxides. The findings provide a feasible approach for precisely intensifying the catalytic activity of a given heterogeneous Lewis acid/base catalyst.

2. Experimental

2.1. Materials

1-Vinylimidazole (99%), 2-bromoethylamine hydrobromide (98%), epichlorohydrin (ECH, 98%), epibromohydrin (98%), epoxypropane (99%), 1,2-epoxybutane (97%), styrene oxide (97.5%), 1,4-phthalaldehyde (98%), 4,4-biphenyldicarboxaldehyde (98%), benzene-1,3,5-tricarbaldehyde (97%) and 2,2'-azoisobutyronitrile (99%) were purchased from Shanghai Titan Technology Co. Ltd. CO_2 (99.99%) and N_2 (99.99%) were purchased from Taiyuan Steel Co. Deionized water was used in all the experiments.

2.2. Synthesis of materials

2.2.1. Homopolymerization of ILs

1-Vinylimidazole (9.41 g, 100 mmol) and 2-bromoethylamine hydrobromate (20.40 g, 100 mmol) were added to 50 mL of anhydrous acetonitrile. The mixture was refluxed at 70 °C under N_2 atmosphere for 24 h. The obtained 1-vinyl-3-ethylamine-imidazolium bromine·hydrobromic acid ([AVIM]Br·HBr) was obtained by centrifugation, washed with anhydrous ethanol (10 mL ×3) and dried in vacuum at 50 °C for 12 h. ^{1}H NMR (400 MHz, DMSO): δ 9.68 (s,1 H), 8.31 (s, 1 H), 8.01 (s, 1 H), 7.39 (q, 1 H), 6.01 (s, 1 H), 5.45 (s, 1 H), 4.54 (m, 2 H), 3.44 (m,2 H). Then, [AVIM]Br·HBr (3.00 g, 10 mmol) and the initiator 2,2'-azodiisobutyronitrile (AIBN, 0.45 g, 2.7 mmol) were dissolved in 15 mL of deionized water and reacted at 70 °C for 8 h. After cooled to room temperature, the homopolymerization of [AVIM]Br·HBr was finished.

2.2.2. Synthesis of dynamic covalent poly(ionic liquids) PAP

The pH of the solution of homopolymerized [AVIM]Br·HBr was adjusted to be a certain value (9, 10 and 11) by using 5 mol·L^{-1} NaOH solution. Then, 1,4-phthalaldehyde (0.67 g, 5 mmol) was added and stirred for 0.5 h. The corresponding products at different pH values were denoted as PAP_{pH9}, PAP_{pH10} and PAP_{pH11}.

2.2.3. Synthesis of dynamic covalent poly(ionic liquids) PBP and PCP

The samples containing different aromatic spacers were synthesized following the similar route of PAP_{pH10}, wherein 1,4-phthalaldehyde (0.67 g, 5 mmol) was replaced by 4,4-biphenyldicarboxaldehyde (1.05 g, 5 mmol) or benzene-1,3,5-tricarbaldehyde (0.53 g, 3.33 mmol). The products were named as PBP_{pH10} and PCP_{pH10}, respectively.

2.3. Characterizations

^{1}H NMR spectra were collected on an Advance plus 400 MHz spectrometer (Bruker). X-ray diffraction (XRD) patterns were recorded on Y2000 (Aolong) in the range of 5°– 80° using Cu Kα radiation at a scanning step of 3°·min^{-1}. Thermogravimetry analysis (TGA) was conducted on a STA 449 F3 Jupiter® instrument (Netzsch) from 30 °C to 800 °C at a heating rate of 10 °C·min^{-1} under N_2 atmosphere. Fourier transform infrared (FT-IR) spectra were recorded on a Tensor 27 spectrometer (Bruker) over KBr pellet in the region of 4000–400 cm^{-1}. N_2 adsorption/desorption isotherms were characterized at 77 K on an ASAP 2020 C volumetric adsorption analyzer (Micromeritics) by Brunner-Emmet-Teller (BET) analytical methods. The samples were activated at 120 °C for 6 h under vacuum condition before test. Elemental analysis (EA) was performed on a Varia EL cube (Elementar). Scanning electron microscopy (SEM) was performed on a JSM-7100 F microscope (JEOL, Japan). The acidity and basicity of the catalysts were determined by temperature-programmed desorption of ammonia (NH_3-TPD) and CO_2 (CO_2-TPD), respectively, by using a TP-5080 adsorption instrument. After the activation of samples at 120 °C for 2 h in a N_2 atmosphere, the samples were adsorbed with NH_3 (or CO_2) at 50 °C for 0.5 h. Then, the samples were purged in N_2 atmosphere at 50 °C for 0.5 h, heated to 150 °C at a rate of 5 °C/min and kept for 1.5 h to finish desorption.

2.4. In-situ diffuse reflectance infrared Fourier transform spectroscopy (in-situ DRIFTS) for CO_2 adsorption and conversion

In-situ DRIFTS was assessed using an attenuated total reflection Fourier transform infrared spectrophotometer with a resolution of 4 cm^{-1} (Nicolet IS10, Thermo Scientific). For CO_2 adsorption, the sample was filled into an *in-situ* IR cell, and N_2 and CO_2 vapors were introduced into the cell. Before the measurement, the samples were purged with N_2 (gas flow: 30 mL·min^{-1}) for 30 min. The baseline was obtained before the sample reaching adsorption equilibrium of N_2. Then CO_2 was purged (gas flow: 15 mL·min^{-1}) for 10 min, and N_2 (gas flow: 10 mL·min^{-1}) was slowly purged until the peaks were unchanged. For the *in-situ* DRIFTS of the reaction of CO_2 and propylene oxide (PO), the catalyst was placed in the IT cell and purged with N_2 (gas flow: 30 mL·min^{-1}) for 30 min at 80 °C before the measurement. Then, CO_2 (gas flow: 5 mL·min^{-1}) was flowed through a washing bottle containing PO and purged into the IR cell for a certain time at 50 °C.

2.5. Catalytic performance evaluation

The mixture of the catalyst (0.125 g) and pre-cooled epoxides (10 mmol) were added into a 10 mL of Schlenk tube connected with a latex balloon. The assembled reactor was kept at 5 °C and purged of air with CO_2 for three times. For the reaction of CO_2 with low-boiling PO, the above operations were done at − 10 °C. Then, 300 mL of CO_2 was filled into the balloon, and the reaction was kept at a certain temperature under stirring at 300 rpm for 24 h. After the reaction, the mixture was cooled to − 10 °C, and remaining CO_2 in the balloon was slowly pressed

into pre-cooled deuterated chloroform ($CDCl_3$). The liquid product was then separated with the catalyst by centrifugation and dissolved in the above $CDCl_3$ solution for ^1H NMR characterization.

The yield of cyclic carbonate was calculated by using Eqs. (1)–(3):

$$\text{Yield}\ (\%) = \text{Conversion} \times \textit{S}\text{electivity} \quad (1)$$

$$\text{Conversion}(\%) = \frac{C_0 - C_t}{C_0} \times 100\% \quad (2)$$

$$\text{Selectivity}(\%) = \frac{C_{carbonate}}{C_0 - C_t} \times 100\% \quad (3)$$

where c_0 and c_t represent the concentrations of epoxide ($mol{\cdot}L^{-1}$) at 0 and t h, respectively, while $c_{carbonate}$ represents the concentration ($mol{\cdot}L^{-1}$) of cyclic carbonate formed at the specified time. The conversion of epoxides and selectivity of cyclic carbonates were calculated from ^1H NMR according to the equations in Fig. S1. The separated catalyst was washed with anhydrous methanol (10 mL × 3), dried at 60 °C for 8 h, and then reused for the next cycling reaction.

2.6. Computational details

The equilibrium geometries of the reactants, products and intermediates were optimized via density functional theory (DFT) calculation by using the B3LYP method and 6–31 G(d) basis set (B3LYP/6–31 G(d)) [35]. The Grimme's DFT-D3 method was applied to correct the van der Waals for all molecules and free radicals. The theoretical FT-IR spectroscopy was calculated by using a scale factor of 0.9613. The beneficial sites for electrophile and nucleophile attack were obtained by using the Fukui function and the dual descriptor [36]. The dual descriptor (Δf) was calculated using Eq. (4) [37].

$$\Delta f = f^+ - f^- = 2q_N - q_{N-1} - q_{N+1} \quad (4)$$

where q_{N+1}, q_N and q_{N-1} are the Hirshfeld charges of the system under anionic (N + 1), neutral (N) and cationic (N-1) states, respectively. The Hirshfeld charges were calculated separately using the Multiwfn software package [37]. The generated wave functions were used for electrostatic potential (ESP) analysis.

The calculation of reaction transition state was performed by using the B3LYP method and 6–31 G(d) basis set (B3LYP/6–31 G(d)) at 323 K. The only virtual frequency in the frequency calculation refers to the presence of transition state. The minimum energy path (MEP) was further confirmed by using the intrinsic reaction coordinate (IRC) method. The sum of the relative energy of catalyst, ECH, and CO_2 was set as 0.00 $kcal{\cdot}mol^{-1}$. The relative energy was calculated according to the reactant energies, which were set as 0.00 $kcal{\cdot}mol^{-1}$, while the barrier height was measured from the corresponding intermediate energy level.

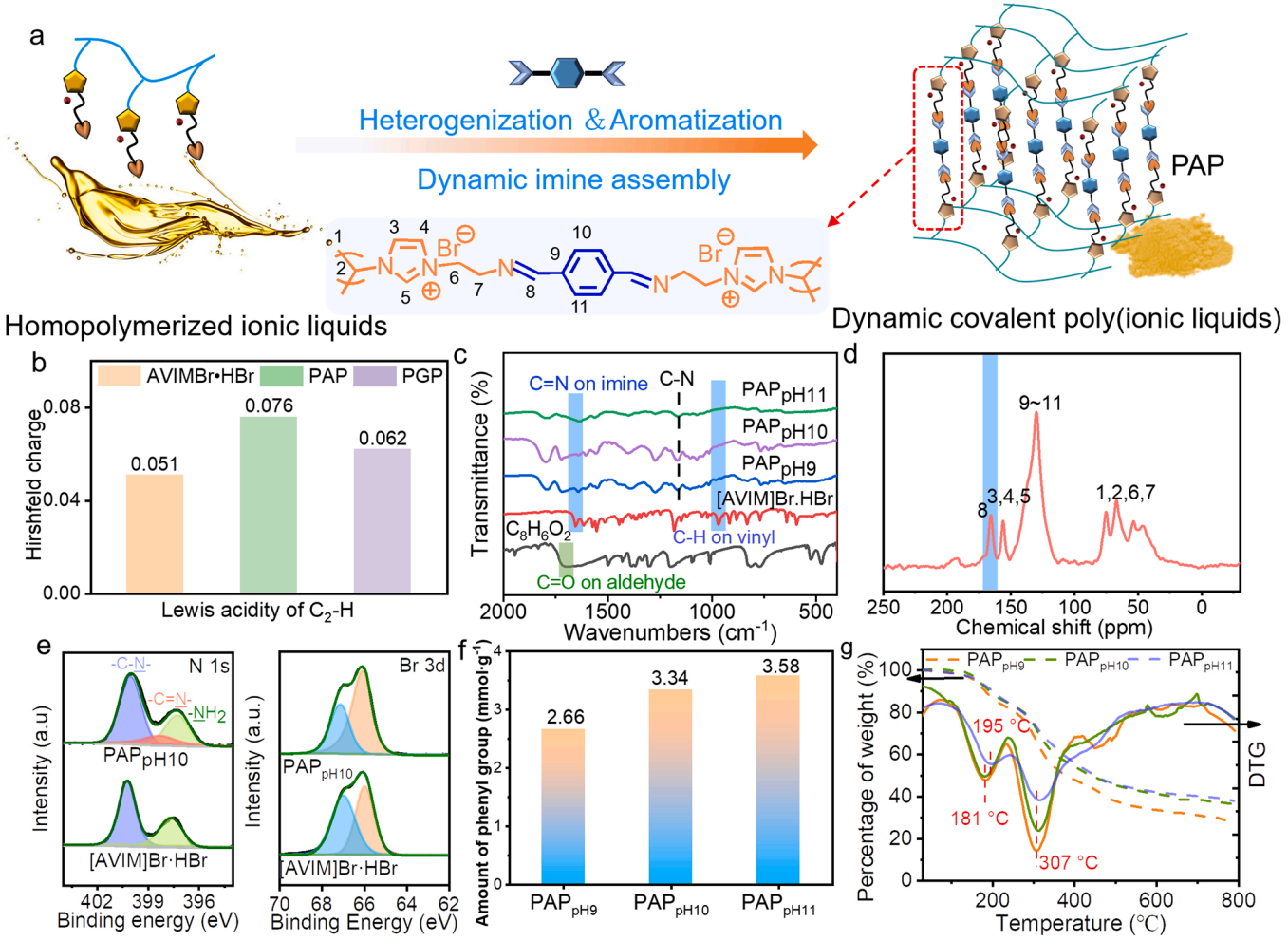

Fig. 1. (a) Schematic illustration for the heterogenization and aromatization of homopolymerized ionic liquids. (b) DFT calculated Hirshfeld charge of C-2 proton on imidazolium ring of [AVIM]Br·HBr and dynamic covalent poly(ionic liquids) (PAP and PGP). (c) FT-IR spectra of [AVIM]Br·HBr, p-benzaldehyde, PAP_{pH9}, PAP_{pH10} and PAP_{pH11}. (d) Solid ^{13}C NMR spectrum of PAP_{pH10}. (e) N 1 S and Br 3d XPS spectra of [AVIM]Br·HBr and PAP_{pH10}. (f) Amount of phenyl group in PAP_{pH9}, PAP_{pH10} and PAP_{pH11}. (g) TGA and DTG profiles for PAP_{pH9}, PAP_{pH10} and PAP_{pH11} in N_2 atmosphere.

3. Results and discussion

3.1. Heterogenization and aromatization of homopolymerized ionic liquids

To achieve the aromatization of homopolymerized ionic liquids, a typical aromatic spacer (i.e., 1,4-phthalaldehyde) has been employed to assembly with amino-functionalized homopolymerized ionic liquids into network through dynamic imine bonding (Fig. 1a). DFT calculation demonstrated the Hirshfeld charge of C-2 proton on imidazolium ring is highly increased from 0.051 to 0.076 with the incorporation of electron-withdrawing aromatic moiety (Fig. 1b), which is just increased to 0.062 when glutaraldehyde (a kind of aliphatic aldehyde) is linked (see PGP in Fig. 1b). This phenomenon indicates the aromatic group enhances the electrophilicity of C-2 proton, which is of high promise for facilitating the ring-opening of epoxides [11–13]. Considering the pH-dependence of dynamic imine bonding [38,39], amino-functionalized polyILs have been assembled with 1,4-phthalaldehyde at different pH values (i.e., pH = 9, 10, 11) and room temperature. It has been observed that homogeneous IL has been successfully transformed into heterogeneous power.

The structures of the resultant dynamic covalent polyILs (named as PAP) have been characterized to confirm the successful polymerization and assembly of amino-functionalized IL. In the FT-IR spectra of the PAP samples (Fig. 1c), the C-H bending vibration band of vinyl group at 962 cm^{-1} disappears, while the characteristic peaks of out-of-plane bending (651, 752 and 853 cm^{-1}) and C-N and C═C stretching (1150 and 1560 cm^{-1}) of the imidazolium ring keep visible, indicating the successful polymerization and incorporation of IL. Particularly, the adsorption band at 1650 cm^{-1} assigned to the C═N bond can be observed, proving the successful reaction of the amino group and aldehyde group [40]. In the solid ^{13}C NMR spectrum of PAP_{pH10} (Fig. 1d), meanwhile, the peak at 168 ppm related to the C═N group can be observed [41]. In the N 1 s XPS profile of AVIM]Br·HBr (Fig. 1e), the two peaks at 400.0 eV and 397.1 eV correspond to the N signals on imidazolium ring and -NH_2 group, respectively. The area percentage of the N 1 s peaks on imidazolium ring and -NH_2 group is 50.5% and 49.5%, respectively (Table S2). A new signal at 398.3 eV appears in the In the N 1 s XPS profile of PAP_{pH10}, signifying the formation of imine bond [42]. Correspondingly, the area percentage of the N 1 s peak on -NH_2 group is significantly decreased to be 13.2%, followed by the

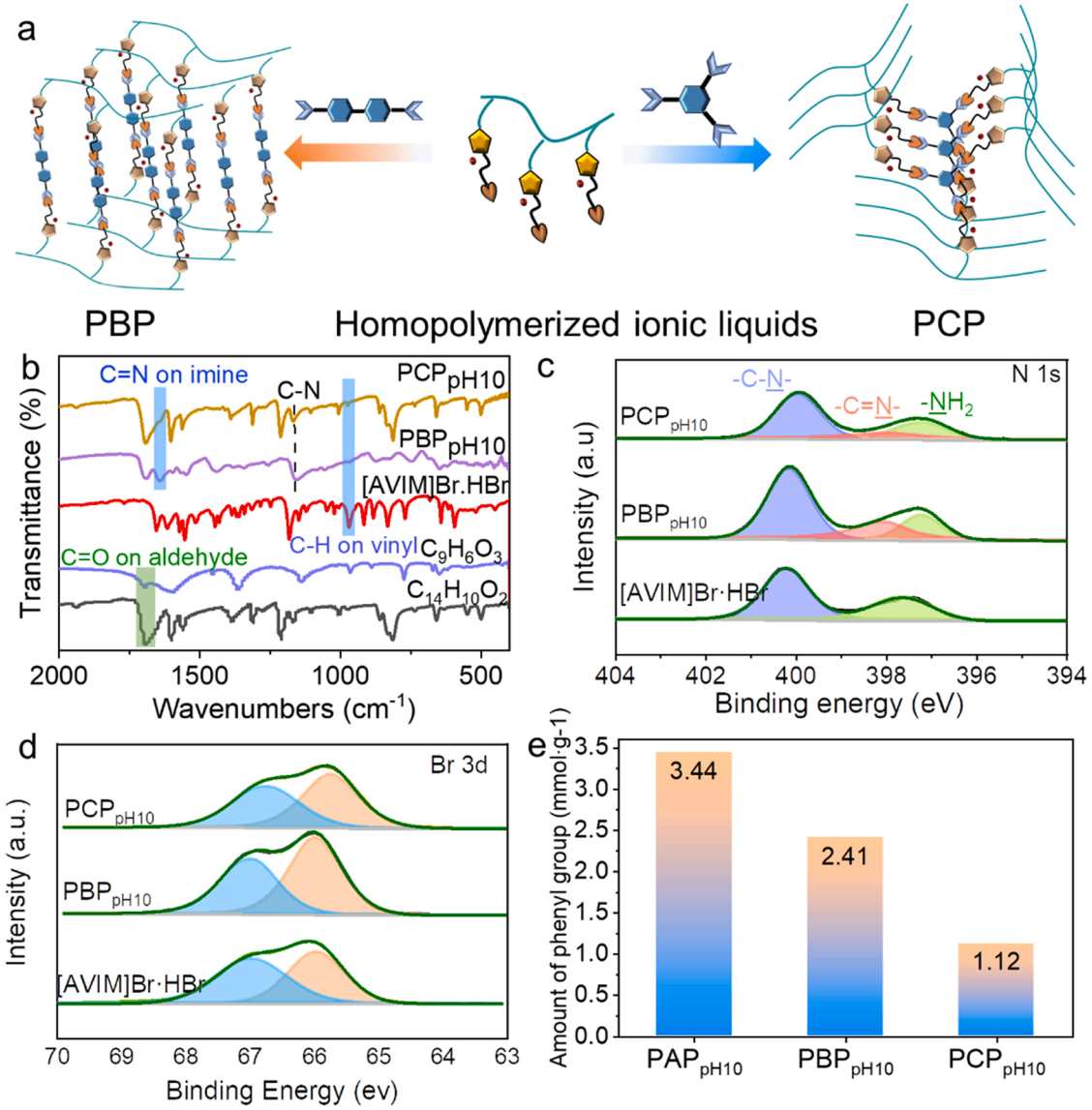

Fig. 2. (a) Schematic illustration for synthesis of PBP_{pH10} and PCP_{pH10}. (b) FT-IR spectra of [AVIM]Br·HBr, 4,4-biphenyldicarboxaldehyde, benzene-1,3,5-tricarbaldehyde, PBP_{pH10} and PCP_{pH10}. (c) N 1 S XPS spectra of [AVIM]Br·HBr, PBP_{pH10} and PCP_{pH10}. (d) Br 3d XPS spectra of [AVIM]Br·HBr, PBP_{pH10} and PCP_{pH10}. (e) Amount of phenyl group in PBP_{pH10} and PCP_{pH10}.

increase of the area percentage of the N 1 s peak on C═N bond to be 35.3%. This result verifies that partial -NH_2 group in [AVIM]Br·HBr has been successfully reacted with aldehyde group to form imine group. While the Br 3d XPS peak position keeps constant after assembly, indicating that Br^- remains at a free state. EA analysis confirmed that the amount of phenyl group is gradually increased from 2.66 to 3.34 and then to 3.58 mmol·g^{-1} with increasing pH from 9.0 to 11.0 (Fig. 1f, detailed calculation is based on Eqs. (S1) and (S2)), which is mainly because a higher pH would facilitate imine assembly [38,39].

To clarify the effect of aromatic moiety on the catalytic performance of dynamic covalent polyILs, a set of control samples have been constructed by using various kinds of aldehyde-based spacers, i.e., glutaraldehyde, 4,4-biphenyldicarboxaldehyde and benzene-1,3,5-tricarbaldehyde (see Fig. 2a). Noting that the employment of glutaraldehyde was failed to afford a heterogeneous power probably due to its flexibility. Similar to PAP_{pH10}, the FT-IR (Fig. 2b) and XPS characterizations (Fig. 2c,d) of the resultant PBP_{pH10} and PCP_{pH10} samples verify the successful assembly of polyILs with aldehyde-based spacers. It has been calculated from EA analysis that the content of the phenyl group is increased from 1.12 mmol·g^{-1} in PCP_{pH10} to 2.41 mmol·g^{-1} in PBP_{pH10} and then to 3.44 mmol·g^{-1} in PAP_{pH10} (Fig. 2e). The much lower content of phenyl group in PBP_{pH10} than the theoretical value is probobaly due to the low solubility of 4,4-biphenyldicarboxaldehyde in water during the synthesis of PBP sample.

The structure and porous properties of the samples have been investigated. SEM and XRD characterizations indicate that the dynamic covalent polymers are amorphous and non-crystalline (Figs. S2 and S3). The pore structures of the materials were analyzed by N_2 adsorption-desorption isotherms. The N_2 adsorption-desorption curves of all the samples present typical H3-type hysteresis loop (Fig. S4), reflecting the wedge-shaped structure [8]." Compared to other PAPs, PAP_{pH10} has a larger specific surface area (33 $m^2·g^{-1}$) and total pore volume (0.081 $cm^3·g^{-1}$) (Table S1). The thermal stability of the catalysts is also one of the critical factors for their practical applications. TGA analysis shows that the samples exhibit good stability with an initial decomposition temperature above 180 ℃, much higher than the catalytic temperature (below 90 ℃). A maximum decomposition temperature around 310 °C can be observed in the samples (Fig. 1g), probably caused by the degradation of imidazole skeleton.

3.2. Metal-/cocatalyst-free and atmospheric CO_2 cycloaddition

The catalytic performances of the dynamic covalent polyILs in the synthesis of cyclic carbonates from CO_2 and epoxides have been evaluated under solvent-/co-catalyst-free conditions. In the typical coupling reaction of CO_2 and epichlorohydrin (ECH), as shown in Figs. 3a and S5, the dynamic covalent polyILs perform good-to-outstanding catalytic activities under extremely mild conditions (1 atm CO_2, T = 50 °C, 24 h). Particularly, a high yield of chloropropene carbonate (CPC) of 94% is afforded over PAP_{pH10}, much more superior than that of bulk polyIL (12%), indicating the beneficial effect of aromatic moiety on the catalytic activity.

The effect of amount of aromatic group on the catalytic performances of dynamic covalent polymers has then been analyzed. The amount of phenyl group decreases following the order of PAP_{pH10} > PBP_{pH10} > PCP_{pH10} > PIL (3.44 vs 2.41 vs 1.12 vs 0 mmol·g^{-1}), and the content of ionic liquid increases correspondingly. It is interestingly found that although the amount of ionic liquid (which contributes the Lewis acidic and basic active sites) is decreased, the catalytic activity in the coupling reaction of CO_2 and epichlorohydrin is increased (Fig. 3b). This result can verify the beneficial effect of aromatic moiety on the strength of Lewis acidity and/or basicity, thus promoting the catalytic activity of

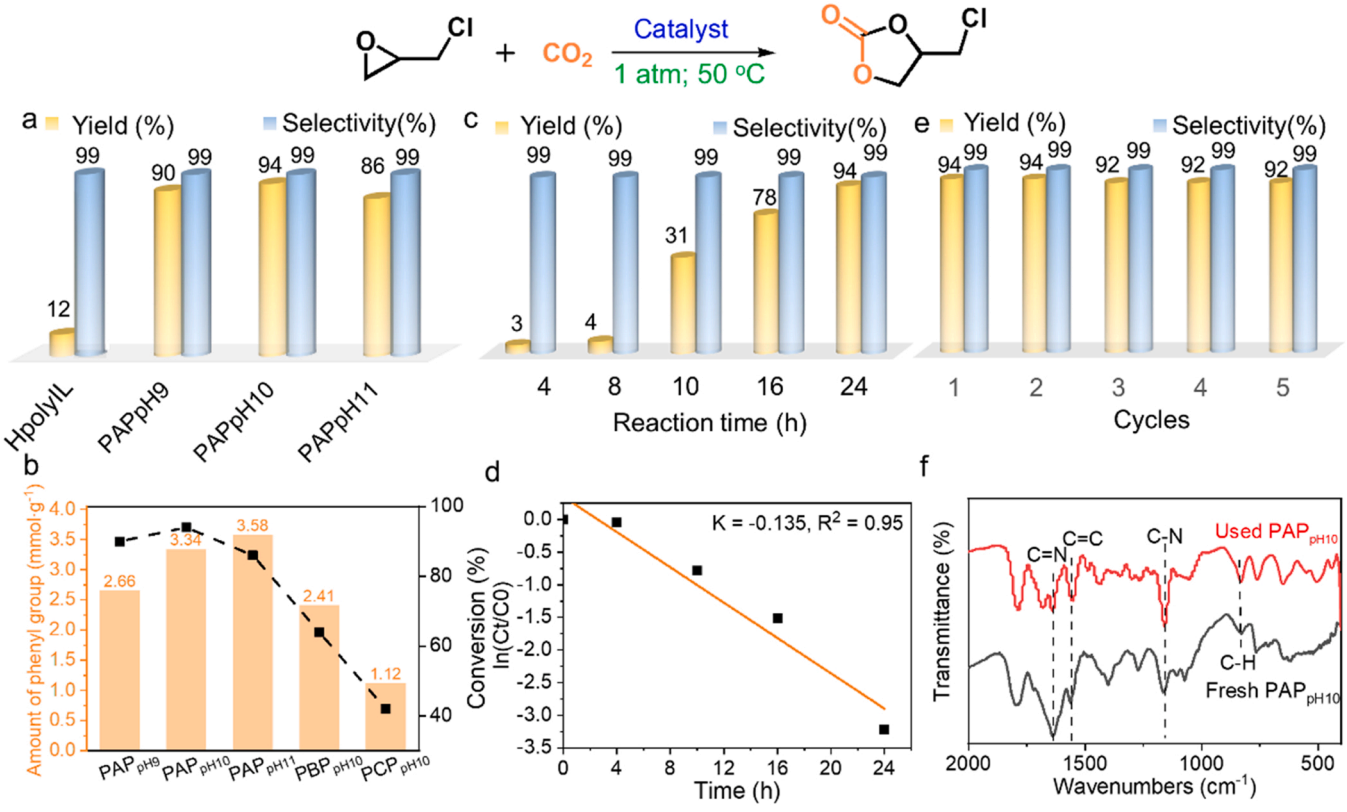

Fig. 3. (a) Catalytic performance of dynamic covalent polyILs (i.e., chloropropylene carbonate yield) in the reaction of CO_2 and ECH. (b) Correlation of catalytic activity with the amount of phenyl group. (c) Catalytic performance of PAP_{pH10} in the reaction of CO_2 and ECH at different time. (d) Kinetic fitting curve of PAP_{pH10}; (e) Cyclic performance of PAP_{pH10}. (f) FT-IR spectra of fresh prepared and recycled PAP_{pH10}. Reaction conditions: (a,b,e) 10 mmol ECH, 0.125 g catalyst, P = 1 bar, t = 24 h; (c,d) 10 mmol ECH, 0.125 g catalyst, P = 1 bar, t = 4, 8, 10, 16, 24 h.

ionic liquid. While for the PAP samples prepared at different pH values, the catalytic activity of PAP_{pH10} is slightly higher than that of PAP_{pH9} and PAP_{pH11} (94% vs 90% vs 86%). This phenomenon implies that an optimized ratio of the aromatic moiety and IL is necessary for balancing their synergy in the catalytic process.

Kinetics is an important index to reflect the nature of the catalytic process. The catalytic activity of PAP_{pH10} as a function of reaction time has then been characterized (Fig. 3c). The reaction rate has been estimated by using Eqs. (S3)–(S5), and the result indicates that the catalytic reaction follows first-order kinetics with a rate constant of 0.135 h^{-1} (Fig. 3d) [43].

The reusability of PAP_{pH10} in the coupling reaction of CO_2 and ECH has then been tested. It can be seen that the catalytic activity of PAP_{pH10} keeps well upon 5 catalytic cycles (Fig. 3e). No obvious mass loss was observed in each cycle and 97 wt% of the initial catalyst was recovered after 5 cycles. SEM, XRD and FT-IR characterizations of the used catalyst show that the structure of PAP_{pH10} remains intact after 5 cycles (Figs. 3f and S6). Meanwhile, the N 1 s and Br 3d XPS signals of used PAP_{pH10} keep consistent with the freshly prepared one, revealing its good catalytic stability. The specific surface area of used PAP_{pH10} is slightly lower than the fresh one (29 $m^2 \cdot g^{-1}$ vs 33 $m^2 \cdot g^{-1}$) (Fig. S6), which is probably caused by the small amount of residual product in the pores. To further confirm the catalyst stability during the catalytic process, we have supplied the catalytic reaction of ECH and CO_2 catalyzed by PAP_{pH10} at a higher temperature (90 ℃) for 24 h. The ^1H NMR spectrum of the resultant liquid product shows that there is no signal of ionic liquid (see Fig. S7), indicating no polyIL catalyst was leached during the reaction process. To further verify the stability of free Br^- ions, the liquid product was dissolved in water and titrated with silver nitrate solution. There is no precipitate observed with the addition of silver nitrate, and the transmittance of the solution detected by UV spectrophotometry is not decreased (see Fig. S8). The slight increase of the transmittance with the addition of silver nitrate is probably because the own pale yellow of CPC is attenuated with the mixture of transparent solution of silver nitrate. The phenomena above confirm there is no leaching of Br- ions and ionic liquids during the catalytic process.

The universality of PAP_{pH10} for the coupling of CO_2 with various epoxides has been detected (Table 1). It can be seen that PAP_{pH10} can catalyze the epoxides with aliphatic alkyl and chloromethyl substituent groups (entries 1–4) into cyclic carbonates with good-to-excellent yields under mild condition (1 atm, 50 °C). A relatively low yield of cyclic carbonates (48%) is afforded in the reaction of CO_2 with phenylethylene oxide caused by the strong conjugative and steric effect of aromatic ring (entry 5) [26]. However, a higher yield (89%) of phenylethylene carbonate can be obtained at 90 ℃ (entry 6). It can be seen that this kind of catalyst performs a great tolerance and high catalytic activity for a variety of epoxides under relatively mild conditions (1 atm, 50–90 ℃).

To evaluate the industrial potential of PAP_{pH10}, the catalytic performance for the coupling reaction of ECH with simulated flue gas (15 vol% CO_2 + 85 vol% N_2) was performed. Considering the temperature of flus gas is generally at the range of 50–120 °C, the catalytic reaction was performed at various temperatures (i.e., 50, 70, 90 and 120 °C). It can be seen in Fig. S9, the CPC yield is 21%, which is increased gradually with the increase of reaction temperature. It's interesting found that the CPC yield can reach up to 92% at 120 °C, demonstrating its great potential for CO_2 conversion in industrial application.

Numerous catalytic systems, including homogeneous and heterogeneous ones, have been developed for the coupling of CO_2 and epoxides, most of which still suffer from high CO_2 pressure and temperature and/or homogeneous cocatalysts [2,7–13,24,44–56]. Kinds of catalysts with relatively high activity (e.g., reaction temperature ≤ 100 ℃, pressure ≤ 20 bar) for different types of epoxides are listed in Table 2. It can be seen that the PAP_{pH10} catalyst developed in this work exhibits comparable and even higher activity than metal-based catalysts (e.g., Entries 2–6, 15). Moreover, PAP_{pH10} catalyst possesses relatively mild preparation and metal-/solvent-/cocatalyst-free nature, thus promoting its competitiveness in practical application. The TON and TOF values of the PAP_{10} catalyst for the reaction of various epoxides and CO_2 have also been calculated (see Table 1). For the calculation of TOF, the mole of active sites in catalyst is obtained from the sum of the Lewis basic and acidic sites determined by CO_2/NH_3 TPD (i.e., 0.32 mmol·g^{-1}, Fig. S10). The TON/TOF values of kinds of catalysts for cycloaddition reactions of epoxides and CO_2 under relatively mild reaction conditions (e.g., reaction temperature ≤ 100 ℃, pressure ≤ 20 bar) are listed in Table S3 [28,57–66]. It can be seen that the TON/TOF values of PAP_{pH10} catalyst are comparable and even higher than metal-based or TBAB-assisted catalysts (e.g., Entries 2–6 and 15), further indicating its superior catalytic activity.

Table 1
Catalytic performance of PAP_{pH10} for the coupling of CO_2 with various epoxides.

Entry	Substrates	Products	T (°C)	P (bar)	t (h)	Yield (%)	Selectivity (%)	TON	TOF (h^{-1})
1			50	1	24	99	99	247.5	10.31
2	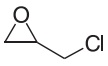	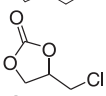	50	1	24	94	99	235.0	9.79
3	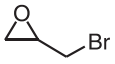	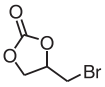	50	1	24	92	99	230.0	9.59
4	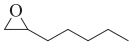	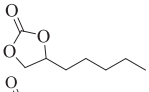	50	1	24	85	99	212.5	8.86
5		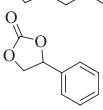	50	1	24	43	99	107.5	4.48
6		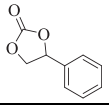	90	1	24	89	99	222.5	9.27

TON = mole of products)/(mole of active sites in catalyst); TOF = mole of products)/(mole of active sites in catalyst)* (reaction time). Mole of active sites in catalyst is obtained from the sum of the basic and acidic sites determined by CO_2/NH_3 TPD.

Table 2
Comparison of the catalytic performance of PAP_{pH10} with previously reported catalysts.

Entry	Catalyst	Substrate	P (bar)	T (°C)	Co-catalyst	t (h)	Yield (%)	Ref.
1	PAP_{pH10}	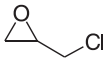	1	50	None	24	94	This work
2	ILs@Al-O-C		1	80	None	24	91	[2]
3	N/O@C		20	100	None	12	90	[10]
4	Co(II)-MOF		10	80	TBAB	3	97	[44]
5	ZnPC-2		15	70	TBAB	8	97.2	[45]
6	Mg-MOF		1	60	None	24	91	[46]
7	COF-SO_3H		1	80	TBAB	24	99	[7]
8	RE-2 f		1	25	TBAI	24	91	[47]
9	PCN-224(Mg)		1	LED light	TBAB	6	≈ 90	[48]
10	Al–N–C		1	Photo	TBAB	16	≈ 91	[49]
11	PAP_{pH10}		1	50	None	24	92	This work
12	Ce-UiO-66-F		1	60	TBAB	4	96	[50]
13	N/O@C		2	100	None	12	99	[10]
14	PAIL-3		5	60	None	2	> 96.3	[51]
15	polyILs@MIL-101		1	70	None	24	85	[24]
16	PAP_{pH10}		1	50	None	24	99	This work
17	[HTMG][His][I]		20	80	None	3	99	[52]
18	PN-CSU23		1	25	TBAB	48	99	[53]
19	PAP_{pH10}		1	90	None	24	89	This work
20	BNCNTs@HMPs-NH_2		1	25	None	24	96	[54]
21	Cu(II)/TD		3	100	None	6	100	[55]
22	PAP_{pH10}	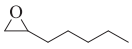	1	50	None	24	85	This work
23	MIL-IL(A)		20	110	None	2	99	[56]

3.3. Effect of aromatic moiety on catalytic mechanism

To verify the beneficial effect of aromatic moiety on the catalytic activity, we compared the reaction activation energy of the cycloaddition of ECH and CO_2 catalyzed by the ionic liquid monomer ([AVIM]Br) and four simplified models of dynamic covalent polyILs, in which two IL monomers are connected with a aliphatic spacer (named as PGP), a phenyl spacer (named as PAP) and a biphenyl spacer (named as PBP) and three IL monomers are connected with a phenyl spacer (named as PCP) by using DFT calculations. The reaction steps (intermediates and transition states) of the cycloaddition of ECH and CO_2 over the three models have been compared (see Figs. 4a and S11). It can be seen that the reaction energy barrier of the cycloaddition of ECH and CO_2 is decreased following the order of PGP > [AVIM]Br > PCP > PAP > PBP (32.32 kcal·mol^{-1} vs 29.73 kcal·mol^{-1} vs 28.14 kcal·mol^{-1} vs 20.95 kcal·mol^{-1} vs 11.16 kcal·mol^{-1}). That is, the reaction energy barrier is increased with the incorporation of aliphatic group on the side-chain of [AVIM]Br and decreased with the incorporation of phenyl group, verifying the catalytic activity of IL can be highly improved with the enhancement of aromaticity.

The detailed activated mechanism during the catalytic process has been demonstrated. Firstly, the acidity and basicity of PAP_{pH10} have been explored by NH_3-TPD and CO_2-TPD, respectively. In both the CO_2-TPD and NH_3-TPD profiles, a broad desorption peak can be observed around 150 ℃ (Fig. S10), implying both basic site and acidic site are present in PAP_{pH10}. The amount of basicity and acidity in PAP_{pH10} is 0.17 mmol·g^{-1} and 0.15 mmol·g^{-1}, respectively. The intermediates and transition states of the cycloaddition of ECH and CO_2 catalyzed by PAP_{pH10} have then been calculated. As is known from Fig. 4a, the ring-opening of epoxides is the rate determining step of the catalytic reaction [10–13]. The C-2 proton on the imidazolium IL can attack the O atom on epoxide through hydrogen bonding interaction and thus weaken the C-O bond (Fig. 4b), which is crucial for facilitating the ring-opening of epoxide [19,20]. It can be seen that the length of hydrogen bond between the C-2 proton on bulk IL monomer and O atom on epoxide is reduced from 2.43 Å to 1.97 Å, 1.91 Å and 1.84 Å with the increase of content of aromatic group, indicating an increased strength of hydrogen bond. As a result, the length of C-O bond on epoxide is increased from 1.44 Å to 1.47 Å, implying a facilitated ring-opening of epoxide [12–14, 16].

To further confirm the catalytic mechanism during the cycloaddition reaction of epoxide and CO_2, in-situ diffuse reflectance infrared Fourier transform spectroscopy (in-situ DRIFTS) of PAP_{pH10} for the reaction of CO_2 and propylene oxide (PO) at different reaction time was performed. As shown in Fig. 4c, the stretching peaks of C═O (1800 cm^{-1}) and O–C–O (1028 cm^{-1}) on the product propylene carbonate (PC) appear with the access of PO and CO_2, indicating the successful conversion of PO and CO_2 into PC. It is interestingly found that the stretching peak of C–H on imidazolium ring (2946 cm^{-1}) shifts significantly to lower frequency (2924 cm^{-1}) during the reaction, followed by the slight shift of the stretching peak of C–H on benzene ring from 974 cm^{-1} to 961 cm^{-1}, which is caused by their hydrogen bonding interaction with O on PO [15]. The C═C stretching peak of benzene/imidazole skeleton also shifts to lower frequency, mainly caused by the electron donating effect of O on PO and/or conjugative effect of O═C═O [30]. Meanwhile, the strengthened C–Br stretching peak (660 cm^{-1}) on the ring-opened intermediate can also be observed. That is, Br^- attacks the less sterically hindered carbon atom of epoxide ring as a nucleophile, thus facilitating the ring-opening of epoxide [26].

As is known, the activation of inert CO_2 is of high promise for boosting its subsequent conversion, which yet remains a great challenge [12]. The active ability of PAP_{pH10} for CO_2 has been visually explored via *in-situ* FT-IR spectroscopy of CO_2 adsorption. In the *in-situ* FT-IR spectroscopy of CO_2 adsorbed on PAP_{pH10} (Fig. 4d), two strong bands for ν_3 antisymmetric stretching at 2359 cm^{-1} and 2331 cm^{-1} with several shoulder peaks can be observed. With N_2 purge for 10 min, most of the above peaks disappear and three large shoulder peaks at the band range of 2331 cm^{-1}∼ 2339 cm^{-1} are still obviously visible with N_2 purge for 10 min. This phenomenon indicates a strong interaction occurs between CO_2 and the corresponding sites. Then, IR patterns of the possible adsorbed sites for CO_2 have been calculated (Fig. 4e). Three sites corresponding to the band at 2331 cm^{-1}, 2335 cm^{-1} and 2339 cm^{-1} have been found (Fig. S12), which are assigned to the O═C═O bending vibrations on phenyl group (Site 1), Br^- ion (Site 2) and both the imine group and phenyl group (Site 3). It is noted that the bond angle of O═C═O has been bended from 180° to 174.4°, 175.0° and 178.5° on Site 1, Site 2 and Site 3, respectively, confirming that CO_2 has been successfully activated [67,68]. Amongst, Br^- ion and imine group act as Lewis basic sites to attack the O atom on CO_2 and the aromatic ring can adsorb and lead to electron transfer and CO_2 bending through π-conjugating interaction [26,30].

In light of the *in-situ* FT-IR and DFT calculation results, it can be

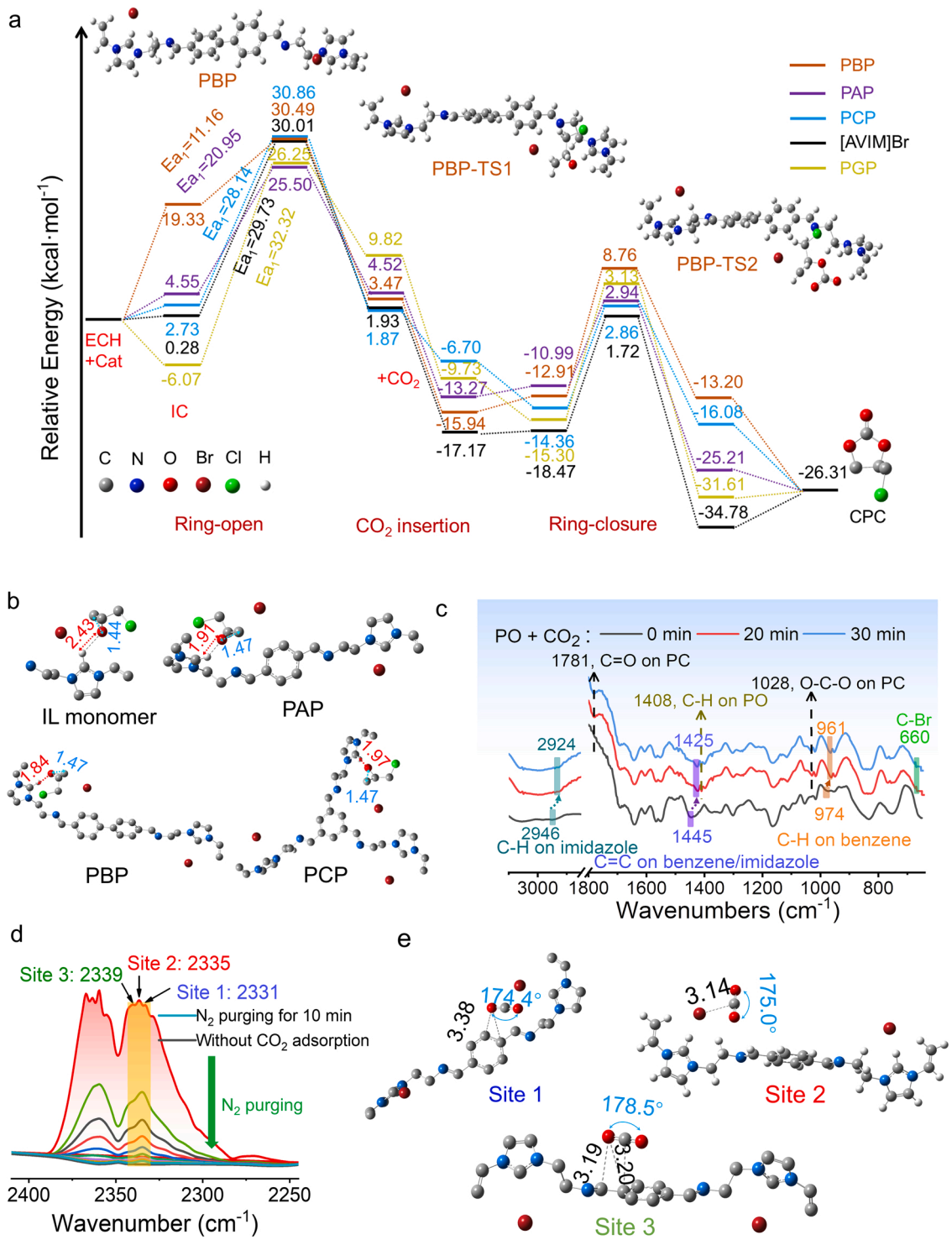

Fig. 4. (a) Relative free energy profiles of the intermediates and transition states of the cycloaddition of ECH and CO_2 catalyzed by ILmonomer [AVIM]Br (black lines) and four simplified models of dynamic covalent polyILs PGP (yellow lines), PAP (purple lines), PBP (red lines) and PCP (blue lines). (b) DFT calculated optimized structures of the reaction intermediates for the ring-opening of ECH catalyzed by bulk ILmonomer [AVIM]Br, PAP, PBP and PCP. (c) *In-situ DRIFTS* spectra of PAP_{pH10} during the reaction of PO with CO_2 at atmospheric pressure and 50 °C for different time (*i. e.*, 0, 20, 30 min). CO_2 flow: mL·min^{-1}. (d) FT-IR patterns of CO_2 adsorbed on PAP_{pH10} in the ν_3 antisymmetric stretching mode regime with N_2 purging. (e) DFT calculated FT-IR patterns and the corresponding optimized structures of CO_2 adsorbed on Site 1, Site 2 and Site 3 of PAP_{pH10}. Bond lengths are reported in Å.

demonstrated that the aromatic group can both activate CO_2 and promote ring-opening of epoxides. The reaction mechanism of CO_2 with epoxides over PAP is thus proposed in Fig. S13. Firstly, the C-2 proton on the imidazolium ring activates O on epoxide through hydrogen bonding interaction, and the nucleophilic Br^- attacks the less sterically hindered carbon atom of epoxide ring. As a result, the ring of epoxide can be opened easily. Meanwhile, the Br^- ion and imine group attack the O atom on CO_2 and the aromatic ring can adsorb CO_2 and lead to electron transfer and CO_2 bending. The activated CO_2 is inserted into the C-Br bonds of the ring-opened intermediate, producing a new intermediate.

Finally, cyclic carbonate is generated via the ring-closing of the intermediate.

4. Conclusion

The heterogenization and aromatization of homogeneous polyILs have been facilely achieved through the dynamic imine assembly of polyILs and aromatic spacers. *In-situ* FT-IR and DFT calculation proved the incorporation of aromatic moiety on IL can facilitate CO_2 activation and promote the hydrogen bonding between C-2 proton on imidazolium ring and O on epoxides synchronously, thus boosting the reaction of CO_2 and epoxides. The structure of the dynamic covalent polyILs can be facilely regulated through the assembly process control, thus offering a feasible approach for promoting the catalytic activity. Superior to most reported heterogeneous catalyst, the resultant dynamic covalent polyILs possess facile preparation, metal-/cocatalyst-free nature, superior activity under extremely mild condition (1 atm, 50–90 ℃, 24 h), outstanding recyclability and great tolerance for a variety of epoxides. This work paves a facile strategy for the tailor-made intensification of the Lewis acidity/basicity of a given heterogeneous catalyst at a molecular level, providing an innovative method to design specific catalysts for energy conversion & utilization and environmental protection.

CRediT authorship contribution statement

Mingyue Qiu: Investigation, Methodology, Visualization, Writing – original draft, Formal analysis. **Jie Li**: Investigation, Formal analysis, Visualization. **Haonan Wu**: Methodology, Visualization. **Yi Huang**: Visualization. **Huijuan Guo**: Formal analysis. **Dan Gao**: Formal analysis. **Qun Yi**: Methodology, Supervision, Conceptualization, Funding acquisition, Writing – review & editing. **Lijuan Shi**: Writing – review & editing, Data curation, Supervision.

Declaration of Competing Interest

The authors declare that they have no known competing financial interests or personal relationships that could have appeared to influence the work reported in this paper.

Data availability

Data will be made available on request.

Acknowledgments

The authors gratefully acknowledge the financial support from the National Natural Science Foundation of China (22272125), Knowledge Innovation Program of Wuhan-Basic Research (2022020801010354), Joint Fund of the Yulin University and the Dalian National Laboratory for Clean Energy (Grant. YLU-DNL Fund 2021021), and Shanxi-Zheda Institute of Advanced Materials and Chemical Engineering (2022SX-TD015).

Appendix A. Supplementary material

Supplementary data associated with this article can be found in the online version at doi:10.1016/j.apcatb.2022.122125.

References

[1] V. Polshettiwar, Dendritic fibrous nanosilica: discovery, synthesis, formation mechanism, catalysis, and CO_2 capture-conversion, Acc. Chem. Res. 55 (2022) 1395–1410.
[2] H.T. Peng, Q.J. Zhang, Y.M. Wang, H.L. Gao, N. Zhang, J. Zhou, L.J. Zhang, Q. Yang, Q.H. Yang, Z.Y. Lu, Atomically dispersed lewis acid sites meet poly(ionic liquid)s networks for solvent-free and co-catalyst-free conversion of CO_2 to cyclic carbonates, Appl. Catal. B Environ. 313 (2022), 121463.
[3] O.B. Ayodele, Rational design of zeolite Y supported oxalate and borohydride ligands functionalized Cu catalysts for CO_2 conversion to specialty chemicals, Appl. Catal. B Environ. 312 (2022), 121381.
[4] T.F. Dong, Y.J. Zheng, G.W. Yang, Y.Y. Zhang, B. Li, G.P. Wu, Crosslinked resin-supported bifunctional organocatalyst for conversion of CO_2 into cyclic carbonates, ChemSusChem 13 (2020) 4121–4127.
[5] S.S. Dhankhar, B. Ugale, C.M. Nagaraja, Co-catalyst-free chemical fixation of CO_2 into fyclic farbonates by using metal-organic frameworks as efficient heterogeneous catalysts, Chem. Asian J. 15 (2020) 2403–2427.
[6] J.F. Kurisingal, Y. Li, Y. Sagynbayeva, R.K. Chitumalla, S. Vuppala, Y. Rachuri, Y. Gu, J. Jang, D.W. Park, Porous aluminum-based DUT metal-organic frameworks for the transformation of CO_2 into cyclic carbonates: a computationally supported study, Catal. Today 352 (2020) 227–236.
[7] G. Singh, C.M. Nagaraja, Highly efficient metal/solvent-free chemical fixation of CO_2 at atmospheric pressure conditions using functionalized porous covalent organic frameworks, J. CO_2 Util. 53 (2021), 101716.
[8] T. Wang, X. Song, H. Xu, M. Chen, J. Zhang, M. Ji, Recyclable and magnetically functionalized metal-organic framework catalyst: IL/Fe_3O_4@HKUST-1 for the cycloaddition reaction of CO_2 with epoxides, ACS Appl. Mater. Interfaces 13 (2021) 22836–22844.
[9] B.H. Cheng, L.J. Deng, J. Jiang, H. Jiang, Catalytic cycloaddition of CO_2 to epoxides by the synergistic effect of acidity and alkalinity in a functionalized biochar, Chem. Eng. J. 442 (2022), 136265.
[10] Q. Han, B. Qi, W. Ren, C. He, J. Niu, C. Duan, Polyoxometalate-based homochiral metal-organic frameworks for tandem asymmetric transformation of cyclic carbonates from olefins, Nat. Commun. 6 (2015) 10007.
[11] K. Chen, H. Li, L. He, Advance and prospective on CO_2 activation and transformation strategy, Chin. J. Org. Chem. 40 (2020) 2195–2207.
[12] L. Guo, K.J. Lamb, M. North, Recent developments in organocatalysed transformations of epoxides and carbon dioxide into cyclic carbonates, Green Chem. 23 (2021) 77–118.
[13] Y.Y. Zhang, G.W. Yang, R. Xie, L. Yang, B. Li, G.P. Wu, Scalable, durable, and recyclable metal-free catalysts for highly efficient conversion of CO_2 to cyclic carbonates, Angew. Chem. Int. Ed. Engl. 59 (2020) 23291–23298.
[14] J.Y. Yang, S.Q. Shi, H.T. Peng, Q.H. Yang, L. Chen, Integration of atomically dispersed Ga sites with C3N4 nanosheets for efficient photo-driven CO_2 cycloaddition, Chem. J. Chin. Univ. 43 (2022) 20220349.
[15] M. Liu, X. Wang, Y. Jiang, J. Sun, M. Arai, Hydrogen bond activation strategy for cyclic carbonates synthesis from epoxides and CO_2: current state-of-the art of catalyst development and reaction analysis, Catal. Rev. 61 (2018) 214–269.
[16] G.W. Yang, Y.Y. Zhang, G.P. Wu, Modular organoboron catalysts enable transformations with unprecedented reactivity, Acc. Chem. Res. 54 (2021) (2021) 4434–4448.
[17] Z.Q. Li, Y.Y. Zhang, Y.J. Zheng, B. Li, G.P. Wu, Insights into thiourea-based bifunctional catalysts for efficient conversion of CO_2 to cyclic carbonates, J. Org. Chem. 87 (2022) 3145–3155.
[18] Y. Zhao, B. Han, Z. Liu, Ionic-liquid-catalyzed approaches under metal-free conditions, Acc. Chem. Res. 54 (2021) 3172–3190.
[19] Y. Qu, Y. Zhao, D. Li, J. Sun, Task-specific ionic liquids for carbon dioxide absorption and conversion into value-added products, Curr. Opin. Green Sustain. 34 (2022), 100599.
[20] G. Chen, J. Zhang, X. Cheng, X. Tan, J. Shi, D. Tan, B. Zhang, Q. Wan, F. Zhang, L. Liu, B. Han, G. Yang, Metal ionic liquids for the rapid chemical fixation of CO_2 under ambient conditions, ChemCatChem 12 (2020) 1963–1967.
[21] W. Dai, Q. Li, J. Long, P. Mao, Y. Xu, L. Yang, J. Zou, X. Luo, Hierarchically mesoporous imidazole-functionalized covalent triazine framework: an efficient metal- and halogen-free heterogeneous catalyst towards the cycloaddition of CO_2 with epoxides, J. CO_2 Util. 62 (2022), 102101.
[22] Y. Sun, X. Jia, H. Huang, X. Guo, Z. Qiao, C. Zhong, Solvent-free mechanochemical route for the construction of ionic liquid and mixed-metal MOF composites for synergistic CO_2 fixation, J. Mater. Chem. A 8 (2020) 3180–3185.
[23] M. Ding, H.L. Jiang, Incorporation of imidazolium-based poly(ionic liquid)s into a metal–organic framework for CO_2 capture and conversion, ACS Catal. 8 (2018) 3194–3201.
[24] R. Luo, Y. Yang, K. Chen, X. Liu, M. Chen, W. Xu, B. Liu, H. Ji, Y. Fang, Tailored covalent organic frameworks for simultaneously capturing and converting CO_2 into cyclic carbonates, J. Mater. Chem. A 9 (2021) 20941–20956.
[25] O. Durak, M. Zeeshan, S. Keskin, A. Uzun, [BMIM][OAc] coating layer makes activated carbon almost completely selective for CO_2, Chem. Eng. J. 437 (2022), 135436.
[26] Q. Yi, T. Liu, X. Wang, Y. Shan, X. Li, M. Ding, L. Shi, H. Zeng, Y. Wu, One-step multiple-site integration strategy for CO_2 capture and conversion into cyclic carbonates under atmospheric and cocatalyst/metal/solvent-free conditions, Appl. Catal. B Environ. 283 (2021), 119620.
[27] Q. Sun, B. Aguila, J. Perman, N. Nguyen, S. Ma, Flexibility matters: cooperative active sites in covalent organic framework and threaded ionic polymer, J. Am. Chem. Soc. 138 (2016) 15790–15796.
[28] Y. Sang, J. Huang, Benzimidazole-based hyper-cross-linked poly(ionic liquid)s for efficient capture and conversion, Chem. Eng. J. 385 (2020), 123973.
[29] G. Li, S. Dong, P. Fu, Q. Yue, Y. Zhou, J. Wang, Synthesis of porous poly(ionic liquid)s for chemical CO_2 fixation with epoxides, Green Chem. 24 (2022) 3433–3460.
[30] Z. Li, L. Sheng, H. Wang, X. Wang, M. Li, Y. Xu, H. Cui, H. Zhang, H. Liang, H. Xu, X. He, Three-dimensional covalent organic framework with ceq topology, J. Am. Chem. Soc. 143 (2021) 92–96.

[31] P. Chakma, D. Konkolewicz, Dynamic covalent bonds in polymeric materials, Angew. Chem. Int. Ed. Engl. 58 (2019) 9682–9695.
[32] J.T. Miao, M.Y. Ge, S.Q. Peng, J. Zhong, Y.W. Li, Z.X. Weng, L.X. Wu, L.H. Zheng, Dynamic imine bond-based shape memory polymers with permanent shape reconfigurability for 4D printing, ACS Appl. Mater. Interfaces 11 (2019) 40642–40651.
[33] X.Y. Ding, G. Li, P. Zhao, E. Jin, C.S. Xiao, X.S. Chen, Injectable self-healing hydrogel wound dressing with cysteine-specific on-demand dissolution property based on tandem dynamic covalent bonds, Adv. Funct. Mater. 31 (2021) 2011230.
[34] N. Zheng, Y. Xu, Q. Zhao, T. Xie, Dynamic covalent polymer networks: a molecular platform for designing functions beyond chemical recycling and self-healing, Chem. Rev. 121 (2021) 1716–1745.
[35] T. Lu, F. Chen, Multiwfn: a multifunctional wavefunction analyzer, J. Comput. Chem. 33 (2012) 580–592.
[36] T. Fievez, N. Sablon, F.D. Proft, P.W. Ayers, P. Geerlings, Calculation of fukui functions without differentiating to the number of electrons. 3. Local fukui function and dual descriptor, J. Chem. Theory Comput. 4 (2008) 1065–1072.
[37] G. Bharathy, J. Christian Prasana, S. Muthu, A. Irfan, F. Basha Asif, A. Saral, S. Aayisha, R. Niranjana, devi, Evaluation of electronic and biological interactions between N-[4-(Ethylsulfamoyl)phenyl]acetamide and some polar liquids (IEFPCM solvation model) with Fukui function and molecular docking analysis, J. Mol. Liq. 340 (2021), 117271.
[38] C.H. Lu, Y.C. Yeh, Fabrication of Multiresponsive magnetic nanocomposite double-network hydrogels for controlled release applications, Small 17 (2021) 2105997.
[39] L. Yang, C. Wang, L. Li, F. Zhu, X. Ren, Q. Huang, Y. Cheng, Y. Li, Bioinspired integration of naturally occurring molecules towards universal and smart antibacterial coatings, Adv. Funct. Mater. 32 (2022) 2108749.
[40] Z. Lu, C. Yang, L. He, J. Hong, C. Huang, T. Wu, X. Wang, Z. Wu, X. Liu, Z. Miao, B. Zeng, Y. Xu, C. Yuan, L. Dai, Asymmetric Hydrophosphonylation of imines to construct highly stable covalent organic frameworks with efficient intrinsic proton conductivity, J. Am. Chem. Soc. 144 (2022) 9624–9633.
[41] M. Zhang, Y. Li, W. Yuan, X. Guo, C. Bai, Y. Zou, H. Long, Y. Qi, S. Li, G. Tao, C. Xia, L. Ma, Construction of flexible amine-linked covalent organic frameworks by catalysis and reduction of formic acid via the eschweiler-clarke reaction, Angew. Chem. Int. Ed. Engl. 60 (2021) 12396–12405.
[42] L. Zheng, L. Liu, J. Yu, P. Shao, Novel trends and applications of natural pH-responsive indicator film in food packaging for improved quality monitoring, Food Control 134 (2022), 108769.
[43] B. Aguila, Q. Sun, X. Wang, E. O'Rourke, A.M. Al-Enizi, A. Nafady, S. Ma, Lower activation energy for catalytic reactions through host-guest cooperation within metal-organic frameworks, Angew. Chem. Int. Ed. Engl. 57 (2018) 10107–10111.
[44] N. Ullah, A. Ramiere, W. Raza, P. Ye, W. Liu, X. Cai, Z. Peng, K.H. Kim, Cobalt-based MOF nanoribbons with abundant O/N species for cycloaddition of carbon dioxide to epoxides, J. Colloid Interface Sci. 623 (2022) 752–761.
[45] L. Kong, Z. Li, H. Hu, J. Zhu, Z. Chen, M. Deng, Y. Ling, P. Li, Y. Jia, Y. Zhou, Reticular chemistry approach to explore the catalytic CO_2-epoxide cycloaddition reaction over tetrahedral coordination Lewis acidic sites in a Rutile-type Zinc-phosphonocarboxylate framework, Chem. Eng. J. 427 (2022), 131759.
[46] R. Das, T. Ezhil, A.S. Palakkal, D. Muthukumar, R.S. Pillai, C.M. Nagaraja, Efficient chemical fixation of CO_2 from direct air under environment-friendly co-catalyst and solvent-free ambient conditions, J. Mater. Chem. A 9 (2021) 23127–23139.
[47] X. Xin, H. Shan, T. Tian, Y. Wang, D. Yuan, H. You, Y. Yao, Conversion of CO_2 into cyclic carbonates under ambient conditions catalyzed by rare-earth metal complexes bearing poly(phenolato) ligand, ACS Sustain. Chem. Eng. 8 (2020) 13185–13194.
[48] R. Das, S.S. Manna, B. Pathak, C.M. Nagaraja, Strategic design of Mg-centered porphyrin metal−organic framework for efficient visible light-promoted fixation of CO_2 under ambient conditions: combined experimental and theoretical investigation, ACS Appl. Mater. Interfaces 14 (2022) 33285–33296.
[49] Q.H. Yang, H.T. Peng, Q.J. Zhang, X. Qian, X. Chen, X. Tang, S. Dai, J.J. Zhao, K. Jiang, Q. Yang, J. Sun, L.J. Zhang, N. Zhang, H.L. Gao, Z.Y. Lu, L. Chen, Atomically dispersed high-density Al–N4 sites in porous carbon for efficient photodriven CO_2 cycloaddition, Adv. Mater. 33 (2021) 2103186.
[50] Q.H. Yang, Y.M. Wang, X. Tang, Q.J. Zhang, S. Dai, H.T. Peng, Y.C. Lin, Z.Q. Tian, Z.Y. Lu, L. Chen, Ligand defect density regulation in metal−organic frameworks by functional group engineering on linkers, Nano Lett. 22 (2022) 838–845.
[51] Y.T. Lei, H.Q. Nimal Gunaratne, L.L. Jin, Design and synthesis of pyridinamide functionalized ionic liquids for efficient conversion of carbon dioxide into cyclic carbonates, J. CO_2 Util. 58 (2022), 101930.
[52] Y. Qu, Y. Chen, J. Sun, Conversion of CO_2 with epoxides to cyclic carbonates catalyzed by amino acid ionic liquids at room temperature, J. CO_2 Util. 56 (2022), 101840.
[53] Y. Lei, Y. Wan, W. Zhong, D. Liu, Z. Yang, Phosphonium-based porous ionic polymer with hydroxyl groups: a bifunctional and robust catalyst for cycloaddition of CO_2 into cyclic carbonates, Polymers 12 (2020) 121–129.
[54] Y.C. Guo, W.J. Chen, L. Feng, Y.C. Fan, C.J.S. Liang, X.M. Wang, X. Zhang, Greenery-inspired nanoengineering of bamboo-like hierarchical porous nanotubes with spatially organized bifunctionalities for synergistic photothermal catalytic CO_2 fixation, J. Mater. Chem. A 10 (2022) 12418–12428.
[55] F. Moeinpour, R. Khalifeh, M. Rajabzadeh, F. Rezaei, S. Javdan, Cu(II)/triazine-based dendrimer as an efficacious recoverable nano-catalyst for CO_2 fixation under solvent-free conditions, Catal. Lett. (2022), https://doi.org/10.1007/s10562-022-03935-2.
[56] M. Bahadori, A. Marandi, S. Tangestaninejad, M. Moghadam, V. Mirkhani, I. Mohammadpoor-Baltork, Ionic liquid-decorated MIL-101(Cr) via covalent and coordination bonds for efficient solvent-free CO_2 conversion and CO_2 capture at low pressure, J. Phys. Chem. C 124 (2020) 8716–8725.
[57] V. Gupta, S.K. Mandal, A microporous metal-organic framework catalyst for solvent-free strecker reaction and CO_2 fixation at ambient conditions, Inorg. Chem. 59 (2020) 4273–4281.
[58] L.G. Ding, B.J. Yao, W.L. Jiang, et al., Bifunctional imidazolium-based ionic liquid decorated UiO-67 type MOF for selective CO_2 adsorption and catalytic property for CO_2 cycloaddition with epoxides, Inorg. Chem. 56 (2017) 2337–2344.
[59] Y.H. Hao, D. Yuan, Y.G. Yao, Metal-free cycloaddition of epoxides and carbon dioxide catalyzed by triazole-bridged bisphenol, ChemCatChem 12 (2020) 4346–4351.
[60] A.K. Ghosh, U. Saha, S. Biswas, Z.A. ALOthman, M.A. Islam, M. Dolai, Anthracene-triazole-dicarboxylate-based Zn(II) 2D metal organic frameworks for efficient catalytic carbon dioxide fixation into cyclic carbonates under solvent-free condition and theoretical study for the reaction mechanism, Ind. Eng. Chem. Res. 61 (2021) 175–186.
[61] Z.F. Dai, Y.Q. Tang, F. Zhang, Y.B. Xiong, S. Wang, Q. Sun, L. Wang, X.J. Meng, L. H. Zhao, F.S. Xiao, Combination of binary active sites into heterogeneous porous polymer catalysts for efficient transformation of CO_2 under mild conditions, Chin. J. Catal. 42 (2021) 618–626.
[62] L.N. Liu, S. Jayakumar, J. Chen, L. Tao, H. Li, Q.H. Yang, C. Li, Synthesis of bifunctional porphyrin polymers for catalytic conversion of dilute CO_2 to cyclic carbonates, ACS Appl. Mater. Interfaces 13 (2021) 29522–29531.
[63] L. He, J.K. Natha, Q. Lin, Robust multivariate metal–porphyrin frameworks for efficient ambient fixation of CO_2 to cyclic carbonates, Chem. Commun. 55 (2019) 412–415.
[64] B.B. Lu, J. Yang, Y.Y. Liu, J.F. Ma, A polyoxovanadate−resorcin[4]arene-based porous metal−organic framework as an efficient multifunctional catalyst for the cycloaddition of CO_2 with epoxides and the selective oxidation of sulfides, Inorg. Chem. 56 (2017) 11710–11720.
[65] S. Yue, H. Qu, X. Song, S. Zang, G. Deng, Hydroxy acid-functionalized ionic liquids as green alternatives for the efficient catalytic conversion of epoxides to cyclic carbonates under solvent and co-catalyst-free conditions, Catal. Sci. Technol. 11 (2021) 6999–7008.
[66] D. Guo, C. Li, J. Zhang, G.Y. Liu, X.G. Luo, F.S. Wu, Metalloporphyrin-based porous organic polymer as an efficient catalyst for cycloaddition of epoxides and CO_2, J. Solid State Chem. 293 (2021), 121770.
[67] L. Ma, W. Zhao, B. Wang, L. Ling, R. Zhang, CO_2 activation and conversion on Cu catalysts: revealing the role of Cu surface defect types in tuning the activity and selectivity, Fuel 313 (2022), 122686.
[68] R. Wang, G. Liu, S.K. Kim, K.H. Bowen, X. Zhang, Gas-phase CO_2 activation with single electrons, metal atoms, clusters, and molecules, J. Energy Chem. 63 (2021) 130–137.